厚生労働科学研究費補助金（医療技術実用化総合研究事業）
分担研究報告書

臨床試験症例登録システムに関する研究

研究分担者　　曽根　美雪　岩手医科大学放射線科　講師

研究要旨
医師主導臨床試験を促進するためのインフラストラクチャーの一つである症例登録システムを、共同利用型のUMIN-INDICEを用いて構築し、その使用評価を行った。

A. 研究目的

Evidence-based medicine (EBM)を実施する上で、臨床試験の実施によるエビデンス創出は、不可欠である。多施設共同臨床試験の推進は、わが国の医療における重要な課題の一つであるが、現時点ではインフラストラクチャーが十分とはいえない。
そこで、Interventional Radiology (IVR)の多施設臨床試験組織である日本腫瘍IVR研究グループ（JIVROSG)において、臨床試験の症例中央登録システムを、大学医療情報ネットワーク(UMIN)のインターネット上の症例登録センター(INDICE)を用いて共同利用型にて構築し、評価した。

B. 研究方法

JIVROSGにおけるUMIN-INDICEの1)運用実績、2)システムの安定性と安全性、3)ユーザの利便性について評価した。

（倫理面への配慮）
システムの構築にあたっては、個人情報保護法および臨床研究における倫理指針に則ったUMINおよびJIVROSGのプライバシー・ポリシーに沿って、研究に参加する患者の個人情報に配慮した。

C. 研究結果

1）運用実績：UMINの汎用症例登録ソフトを試験ごとにカスタマイズしたもの（登録受付は24時間、症例番号、ランダム化割付は即時に画面上表示）を使用。登録は研究者限定ウエブ・ページから行い、15の臨床試験において、月間3-10症例が登録された。トラブルは、症例登録一時停止の不備(1回)、パスワード紛失による代理登録(3回)があった。
2）システムの安定性と安全性：UMINでは、専門の技術者がサーバの管理・保守を行い、ファイヤウォール、侵入検知、暗号通信、データのバックアップおよび遠隔地保管等を行っている。トラブルは、症例登録一時停止の不備(1回)、パスワード紛失による代理登録(3回)があった。
3）システムの安定性と安全性：UMINでは、専門の技術者がサーバの管理・保守を行い、ファイヤウォール、侵入検知、暗号通信、データのバックアップおよび遠隔地保管等を行っている。これに加え、登録時に入力された患者個人情報はアクセス制限のあるファイルに保管し、以後の運用は症例番号のみで行うシステムとした。これらにより、個人情報の漏洩、紛失に関わるインシデントはなかった。
4）ユーザの利便性：登録経験者41名における満足度調査では、不満足の評価はなかった。

D. 考察

UMIN-INDICEを用いた共同利用型の臨床試験患者登録システムにより、安全かつ利便性の高い患者登録が可能であった。直接比較は行っていないものの、研究独自、ないしは研究グループで症例登録センターを構築するのに比較して、安価であり、安全性の実績は他の利用者にて示されているため、信頼性の高いシステムと考えられる。

E. 結論

UMIN-INDICEは、1)運用実績、2)システムの安定性と安全性、3)ユーザの利便性の点で、多施設共同臨床試験の症例登録システムに有用と判断された。

F. 研究発表

1. 論文発表

1. Sone M, Kato K, Hirose A, et al. Impact of Multislice CT Angiography on Planning of Radiological Catheter Placement for Hepatic Arterial Infusion Chemotherapy. Cardiovasc Intervent Radiol. 31: 91-97, 2008

2. 苫米地牧子、加藤健一、曽根美雪. 18G semi-automatic 針による胸部 CT ガイド下生検：検査成績と合併症の検討. 岩手医誌 60(2); 105-111, 2008

3. Tomabechi M, Kato K, Sone M, et al. Cerebral air embolism treated with hyperbaric oxygen therapy following percutaneous transthoracic computed tomography-guided needle biopsy of the lung. Radiat Med. 2008 Jul;26(6):379-83. 2008

4. 加藤健一、曽根美雪、中里龍彦、他. 進行胆嚢癌・胆嚢癌肝転移に対する肝動注療法. 癌と化学療法 Jpn J Cancer Chemother 35(10): 1691-1695. 2008

2. 学会発表

1. 曽根美雪. 多施設共同研究「埋め込み型中心静脈ポートシステムの不具合に関する調査研究の中間解析結果の解釈. (2008/1/10-11, 第32回リザーバー研究会、舞浜)

2. 曽根美雪. シンポジウム4 "放射線医療における男女共同参画" 放射線科における男女共同参画. (2008/4/6, 第67回日本医学放射線学会総会、横浜)

3. Sone M, Kato K, Tomabechi M, et al. Porous gelatin particles for uterine artery embolization (UAE) in swine: Experimental study of acute effects comparing 1mm and 2mm particles. (2008/5/14-16, ISIR & JSIR 2008, Karuizawa, Japan)

4. 曽根美雪. リフレッシャーコース IVR: IVRにおける臨床試験. (2008/10/24, 第44回 日本医学放射線学会秋季臨床大会、郡山)

H. 知的財産権の出願・登録状況

(予定を含む。)

1. 特許取得
なし

2. 実用新案登録
なし

3. その他
なし

Note: This copy is for your personal, non-commercial use only. To order presentation-ready copies for distribution to your colleagues or clients, use the *Radiology* Reprints form at the end of this article.

Patlak Plot Analysis for Assessment of Single-Kidney Glomerular Filtration Rate with Dynamic CT

From
Yoshito Tsushima, MD, Ayako Taketomi-Takahashi, MD, and Keigo Endo, MD
Department of Diagnostic Radiology and Nuclear Medicine, Gunma University Hospital, 3-39-15 Showa-machi, Maebashi, Gunma 371-8511, Japan
e-mail: *yoshito@xa2.so-net.ne.jp*

Editor:

We read the article by Dr Daghini and colleagues (1) in the February 2007 issue of *Radiology* with great interest. For assessment of single-kidney glomerular filtration rate (GFR) of pigs at computed tomography (CT), the authors compared three mathematic models—original Patlak method, modified Patlak method, and gamma variate modeling—and concluded that the latter two methods may potentially have clinical usefulness. However, the GFR calculated by using the modified Patlak method was overestimated, and the lack of a significant correlation between GFR measured with the original Patlak method and reference value was not consistent with findings of previous studies (2–4).

There are several important assumptions to be kept in the Patlak plot method, and the authors suggested that a sampling time limited to the early phase of the dynamic CT scan and selecting regions of interest (ROIs) limited to the renal cortex would solve these limitations for the most part (1). However, it is very important to define which data points are to be used for calculation, since the Patlak plot is nonlinear in shape (steep in early phase and later less so). According to findings of a study on magnetic resonance in humans (5), the best time window for GFR calculation was 40–110 seconds postaortic rise. While ROI selection including only the renal cortex may provide better results, we suspect that the time window for the Patlak plot may be more important.

There is another important assumption of the Patlak plot: The blood iodine concentrations must be equal at all data sampling regions. To make the difference as small as possible, a slower injection of a smaller amount of contrast medium may be better (2,3). In the study by Dr Daghini and colleagues (1), highly concentrated contrast medium was administered via a central venous catheter as an extremely rapid bolus injection (15 mL/sec). It seems unlikely that the assumption of equal blood iodine concentrations can be met in this case. Injection via a central venous catheter is also impractical in a clinical environment.

Nevertheless, further detailed and careful investigations in human kidneys are necessary for applying this attractive technique to clinical practice. We encourage studies concerning *(a)* the best ROI setting, *(b)* the appropriate time window for calculation, *(c)* the best amount of contrast medium and speed of venous injection, and *(d)* the effect of the third space (interstitium), particularly in diseased kidneys.

References

1. Daghini E, Juillard L, Haas JA, Krier JD, Romero JC, Lerman LO. Comparison of mathematic models for assessment of glomerular filtration rate with electron-beam CT in pigs. Radiology 2007;242:417–424.
2. Tsushima Y, Blomley MJ, Kusano S, Endo K. Use of contrast-enhanced computed tomography to measure clearance per unit renal volume: a novel measurement of renal function and fractinal vascular volume. Am J Kidney Dis 1999;33:754–760.
3. Tsushima Y, Blomley MJ, Okabe K, Tsuchiya K, Aoki J, Endo K. Determination of glomerular filtration rate per unit renal volume using computerized tomography: correlation with conventional measures of total and divided renal function. J Urol 2001;165:382–385.
4. Miles KA, Leggett DA, Bennett GA. CT derived Patlak images of the human kidney. Br J Radiol 1999;72:153–158.
5. Hackstein N, Heckrodt J, Rau WS. Measurement of single-kidney glomerular filtration rate using a contrast-enhanced dynamic gradient-echo sequence and the Rutland-Patlak plot technique. J Magn Reson Imaging 2003;18:714–725.

Response

From
Elena Daghini, MD,* and Lilach O. Lerman, MD, PhD*†
Department of Internal Medicine, Divisions of Nephrology and Hypertension* and Cardiovascular Diseases,† Mayo Clinic College of Medicine, 200 First St SW, Rochester, MN 55905
e-mail: *lerman.lilach@mayo.edu*

We thank Dr Tsushima and colleagues for their interest in our work and for their thoughtful comments.

As mentioned in our article (1) and by Dr Tsushima and colleagues, application of the Patlak method to CT imaging involves several considerations regarding image acquisition and analysis. Our study demonstrated that experimental estimation of GFR by using the Patlak method could be improved by selecting an ROI in the renal cortex, in which filtration takes place, and the time window during which it occurs during first-pass of a contrast medium bolus. As Dr Tsushima and colleagues implied, the selected injection protocol certainly influences the optimal time window for sampling. Both peripheral and superior vena cava injections allow complete indicator mixing with blood during its transition through the cardiac chambers (2). However, as Dr Tsushima and colleagues indicated, slow peripheral infusion and gradual accumulation of contrast medium require sampling at later time points. Nevertheless, selection of an early time window corresponding to the rapid central venous injection in our study complied with the requisite for the indicator to be at least temporarily trapped in the ROI during sampling.

Another feature of the first-pass approach is that immediate changes in cortical enhancement result mainly from contrast medium filtration to the proximal tubule. Hence, this approach may be less susceptible to artifacts consequent to diuresis, like dilution or faster transit of intratubular contrast material, which are largely observed at later time points dur-

ing translocation along the tubular system. In fact, the use of diuretic challenge may partly account for the poorer correlation between the original Patlak method and reference GFR values observed in our study (1), but not in previous studies. Furthermore, our study included mostly healthy animals with a limited range of GFR values, whereas evaluation of human subjects with renal disease (3) may improve the observed relationship by extending this range.

Indeed, we agree with Dr Tsushima and colleagues that peripheral contrast agent injections are more practical for routine clinical use, and we encourage refining the Patlak method to decrease its invasiveness and ensure utility; for example, selection of a cortical ROI in conjunction with peripheral injections may suffice to increase the versatility of this approach. Clearly, studies are needed to optimize application of the Patlak technique to renal functional CT studies. We hope that continued fruitful discussion would facilitate and expedite such studies.

References

1. Daghini E, Juillard L, Haas JA, Krier JD, Romero JC, Lerman LO. Comparison of mathematic models for assessment of glomerular filtration rate with electron-beam CT in pigs. Radiology 2007;242:417–424.

2. Iwasaki T, Ritman EL, Fiksen-Olsen MJ, Romero JC, Knox FG. Renal cortical perfusion: preliminary experience with the dynamic spatial reconstructor (DSR). Ann Biomed Eng 1985;13:259–271.

3. Tsushima Y, Blomley MJ, Okabe K, Tsuchiya K, Aoki J, Endo K. Determination of glomerular filtration rate per unit renal volume using computerized tomography: correlation with conventional measures of total and divided renal function. J Urol 2001;165:382–385.

Radiology 2007

This is your reprint order form or pro forma invoice

(Please keep a copy of this document for your records.)

Reprint order forms and purchase orders or prepayments must be received 72 hours after receipt of form either by mail or by fax at 410-820-9765. It is the policy of Cadmus Reprints to issue one invoice per order. **Please print clearly.**

Author Name _____
Title of Article _____
Issue of Journal _____ Reprint # _____ Publication Date _____
Number of Pages _____ KB # _____ Symbol Radiology
Color in Article? Yes / No (Please Circle)

Please include the journal name and reprint number or manuscript number on your purchase order or other correspondence.

Order and Shipping Information

Reprint Costs (Please see page 2 of 2 for reprint costs/fees.)

_____ Number of reprints ordered $_____
_____ Number of color reprints ordered $_____
_____ Number of covers ordered $_____
Subtotal $_____
Taxes $_____

(Add appropriate sales tax for Virginia, Maryland, Pennsylvania, and the District of Columbia or Canadian GST to the reprints if your order is to be shipped to these locations.)

First address included, add $32 for each additional shipping address $_____

TOTAL $_____

Shipping Address (cannot ship to a P.O. Box) Please Print Clearly

Name _____
Institution _____
Street _____
City _____ State _____ Zip _____
Country _____
Quantity _____ Fax _____
Phone: Day _____ Evening _____
E-mail Address _____

Additional Shipping Address* (cannot ship to a P.O. Box)

Name _____
Institution _____
Street _____
City _____ State _____ Zip _____
Country _____
Quantity _____ Fax _____
Phone: Day _____ Evening _____
E-mail Address _____

** Add $32 for each additional shipping address*

Payment and Credit Card Details

Enclosed: Personal Check _____
Credit Card Payment Details _____

Checks must be paid in U.S. dollars and drawn on a U.S. Bank.

Credit Card: __ VISA __ Am. Exp. __ MasterCard
Card Number _____
Expiration Date _____
Signature: _____

Please send your order form and prepayment made payable to:

Cadmus Reprints
P.O. Box 751903
Charlotte, NC 28275-1903

Note: Do not send express packages to this location, PO Box.
FEIN #:541274108

Invoice or Credit Card Information

Invoice Address **Please Print Clearly**

Please complete Invoice address as it appears on credit card statement

Name _____
Institution _____
Department _____
Street _____
City _____ State _____ Zip _____
Country _____
Phone _____ Fax _____
E-mail Address _____

Cadmus will process credit cards and *Cadmus Journal Services* will appear on the credit card statement.

If you don't mail your order form, you may fax it to 410-820-9765 with your credit card information.

Signature _____ Date _____

Signature is required. By signing this form, the author agrees to accept the responsibility for the payment of reprints and/or all charges described in this document.

RB-9/22/06

Radiology 2007

Black and White Reprint Prices

Domestic (USA only)						
# of Pages	50	100	200	300	400	500
1-4	$213	$228	$260	$278	$295	$313
5-8	$338	$373	$420	$453	$495	$530
9-12	$450	$500	$575	$635	$693	$755
13-16	$555	$623	$728	$805	$888	$965
17-20	$673	$753	$883	$990	$1,085	$1,185
21-24	$785	$880	$1,040	$1,165	$1,285	$1,413
25-28	$895	$1,010	$1,208	$1,350	$1,498	$1,638
29-32	$1,008	$1,143	$1,363	$1,525	$1,698	$1,865
Covers	$95	$118	$218	$320	$428	$530

International (includes Canada and Mexico)						
# of Pages	50	100	200	300	400	500
1-4	$263	$275	$330	$385	$430	$485
5-8	$415	$443	$555	$650	$753	$850
9-12	$563	$608	$773	$930	$1,070	$1,228
13-16	$698	$760	$988	$1,185	$1,388	$1,585
17-20	$848	$925	$1,203	$1,463	$1,705	$1,950
21-24	$985	$1,080	$1,420	$1,725	$2,025	$2,325
25-28	$1,135	$1,248	$1,640	$1,990	$2,350	$2,698
29-32	$1,273	$1,403	$1,863	$2,265	$2,673	$3,075
Covers	$148	$168	$308	$463	$615	$768

Minimum order is 50 copies. For orders larger than 500 copies, please consult Cadmus Reprints at 800-407-9190.

Reprint Cover

Cover prices are listed above. The cover will include the publication title, article title, and author name in black.

Shipping

Shipping costs are included in the reprint prices. Domestic orders are shipped via UPS Ground service. Foreign orders are shipped via a proof of delivery air service.

Multiple Shipments

Orders can be shipped to more than one location. Please be aware that it will cost $32 for each additional location.

Delivery

Your order will be shipped within 2 weeks of the journal print date. Allow extra time for delivery.

Color Reprint Prices

Domestic (USA only)						
# of Pages	50	100	200	300	400	500
1-4	$218	$233	$343	$460	$579	$697
5-8	$343	$388	$584	$825	$1,069	$1,311
9-12	$471	$503	$828	$1,196	$1,563	$1,935
13-16	$601	$633	$1,073	$1,562	$2,058	$2,547
17-20	$738	$767	$1,319	$1,940	$2,550	$3,164
21-24	$872	$899	$1,564	$2,308	$3,045	$3,790
25-28	$1,004	$1,035	$1,820	$2,678	$3,545	$4,403
29-32	$1,140	$1,173	$2,063	$3,048	$4,040	$5,028
Covers	$95	$118	$218	$320	$428	$530

International (includes Canada and Mexico))						
# of Pages	50	100	200	300	400	500
1-4	$268	$280	$412	$568	$715	$871
5-8	$419	$457	$720	$1,022	$1,328	$1,633
9-12	$583	$610	$1,025	$1,492	$1,941	$2,407
13-16	$742	$770	$1,333	$1,943	$2,556	$3,167
17-20	$913	$941	$1,641	$2,412	$3,169	$3,929
21-24	$1,072	$1,100	$1,946	$2,867	$3,785	$4,703
25-28	$1,246	$1,274	$2,254	$3,318	$4,398	$5,463
29-32	$1,405	$1,433	$2,561	$3,788	$5,014	$6,237
Covers	$148	$168	$308	$463	$615	$768

Tax Due

Residents of Virginia, Maryland, Pennsylvania, and the District of Columbia are required to add the appropriate sales tax to each reprint order. For orders shipped to Canada, please add 7% Canadian GST unless exemption is claimed.

Ordering

Reprint order forms and purchase order or prepayment is required to process your order. Please reference journal name and reprint number or manuscript number on any correspondence. You may use the reverse side of this form as a proforma invoice. Please return your order form and prepayment to:

Cadmus Reprints
P.O. Box 751903
Charlotte, NC 28275-1903

Note: Do not send express packages to this location, PO Box.
FEIN #:541274108

Please direct all inquiries to:

Rose A. Baynard
800-407-9190 (toll free number)
410-819-3966 (direct number)
410-820-9765 (FAX number)
baynardr@cadmus.com (e-mail)

Reprint Order Forms and purchase order or prepayments must be received 72 hours after receipt of form.

Ann Nucl Med (2008) 22:83–86
DOI 10.1007/s12149-007-0076-1

CASE REPORT

Clinicopathological presentation of varying ^{18}F-FDG uptake and expression of glucose transporter 1 and hexokinase II in cases of hepatocellular carcinoma and cholangiocellular carcinoma

**Bishnuhari Paudyal · Noboru Oriuchi · Pramila Paudyal
Yoshito Tsushima · Tetsuya Higuchi
Mitsuyuki Miyakubo · Tomohiro Ishikita
Takashi Nakajima · Keigo Endo**

Received: 10 May 2007 / Accepted: 8 September 2007
© The Japanese Society of Nuclear Medicine 2008

Abstract We report the results of ^{18}F-fluorodeoxyglucose positron emission tomography (FDG PET) and immunohistochemical staining of glucose transporter 1 (Glut-1) and hexokinase II (HK-II) in patients with hepatocellular carcinoma (HCC) and cholangiocellular carcinoma (CCC) to observe the variation in ^{18}F-FDG uptake and variation in expression of Glut-1 and HK-II in these hepatic tumors. In the case of HCC, moderate ^{18}F-FDG uptake and strong expression of HK-II were detected, whereas Glut-1 was not expressed. Conversely, CCC showed high ^{18}F-FDG uptake and increased expression of Glut-1 but HK-II was not expressed. The variation in the ^{18}F-FDG uptake and expression of Glut 1 and HK-II in HCC and CCC might be owing to the difference in origin and the different mechanisms involved in glucose uptake, rate of glucose transporters, and hexokinase activity involved in the glycolytic pathway.

Keywords ^{18}F-FDG PET · Glucose transporter 1 · Hexokinase II · Hepatocellular carcinoma · Cholangiocellular carcinoma

B. Paudyal (✉) · N. Oriuchi · P. Paudyal · Y. Tsushima · T. Higuchi · M. Miyakubo · T. Ishikita · K. Endo
Department of Diagnostic Radiology and Nuclear Medicine, Gunma University Graduate School of Medicine, 3-39-22 Showa-machi, Maebashi, Gunma 371-8511, Japan
e-mail: paudyal@med.gunma-u.ac.jp

P. Paudyal · T. Nakajima
Department of Tumor Pathology, Gunma University Graduate School of Medicine, Maebashi, Gunma, Japan

Introduction

Hepatocellular carcinoma (HCC) and cholangiocellular carcinoma (CCC) are the most common primary hepatic tumors and are prevalent in Asia and Africa [1, 2]. HCC arises from the hepatic parenchyma. CCC arises from the ductal epithelium of the biliary tree, either within the liver or more commonly from the extrahepatic bile duct. Surgical resection is the only definitive treatment strategy for both types of tumor. Unfortunately, not all patients are candidates for surgery for various reasons [3, 4]. Therefore, early diagnosis and accurate staging are essential for the appropriate management of patients.

Many studies have focused on the expression of glucose transporter 1 (Glut-1) and hexokinase II (HK-II) activities as correlated with ^{18}F-fluorodeoxyglucose (FDG) uptake in the various types of tumors [5–7]. It has been reported that overexpression of Glut-1 and HK-II was associated with enhanced tumor aggressiveness and poor survival [5–10]. Until now, only few studies on the importance of ^{18}F-FDG PET in CCC and HCC [3, 4, 11, 12] have been reported in which ^{18}F-FDG PET could identify the primary tumor site accurately with a sensitivity of 90% and above in CCC [3, 4]. The findings of these studies confirm the high sensitivity of PET in assisting the detection of CCC. However, the detection of primary HCC is still controversial [11–13]. This prompted us to discuss here cases of HCC and CCC, which showed variation in the ^{18}F-FDG uptake and in the expression of Glut-1 and HK–II as determined by immunohistochemical examination.

Methods

^{18}F-FDG PET imaging was performed with a dedicated scanner (SET2400W, Shimadazu, Kyoto, Japan) as we described earlier [14]. Patients fasted for 6h prior to ^{18}F-FDG PET scanning. The data were acquired by the simultaneous emission–transmission methods with a rotating external source (^{68}Ge) at 60min following the injection of 5MBq/kg body weight. Five bed positions (100cm) from the head to the thigh were imaged for 8min per position. The attenuation-corrected transaxial images were reconstructed using an ordered subsets expectation maximization algorithm into a 128 × 128 matrix.

Immunohistochemical examination was performed on the paraffin-embedded tissue section using the streptoavidin biotin method. The sections were deparaffinized, rehydrated, and incubated with hydrogen peroxide, and pretreated in a 0.01mol/l citrate buffer using a microwave oven at 98°C for 15min. The sections were then incubated with the primary polyclonal antibody at a dilution of 1:1000 for Glut-1 (DakoCytomation, Carpinteria, CA, USA) and a dilution of 1:3000 for HK-II (Chemicon International, Temecula, CA, USA) in 1% bovine serum albumin at 4°C overnight. Signals were detected using an En Vision Kit (DakoCytomation).

Case report

A 69-year-old woman was admitted to our hospital owing to upper abdominal pain and fever. An enhanced computed tomography (CT) showed dilation of the left intrahepatic bile duct and a small enhanced mass lesion at the hepatic hilum (Fig. 1c). CCC was suspected from the CT findings and elevated serum carbohydrate antigen 19-9 level of 111ng/ml. Hepatitis B virus and hepatitis C virus were negative. ^{18}F-FDG PET was performed for clinical staging and confirmation of malignant disease prior to surgery. ^{18}F-FDG PET showed a focal uptake in the tumor located at the hepatic hilum (Fig. 1a, b). A histopathological examination followed by surgery revealed ill-defined infiltrating tumor cells, showing proliferation of irregular ductal formation. These findings confirmed the final diagnosis as moderately differentiated CCC with T2N1M0.

In another case, a 62-year-old woman with hepatitis C viral infection underwent diagnostic workup for a hepatic tumor. An enhanced CT examination revealed a hypervascular tumor of 28mm in the fifth segment of the liver (Fig. 2b, c). Tumor markers of alpha fetoprotein and PIVKA II were elevated to 21.2ng/ml and 308ng/ml, respectively. ^{18}F-FDG PET showed a slightly increased uptake of ^{18}F-FDG in the tumor when compared with normal liver parenchyma (Fig. 2a). A histopathological examination followed by surgery revealed proliferation of infiltrating cells with cellular atypia. These cells had variously sized large nuclei, and formed a trabecular arrangement. These findings confirmed the final diagnosis as moderately differentiated HCC with T3N0M0.

Discussion

Although most malignant tumors show increased ^{18}F-FDG uptake and high expression of Glut-1 and HK-II [5–7, 15], the present case of HCC showed moderate uptake and strong expression of HK-II (Fig. 2a–f), whereas Glut-1 was not expressed. An earlier study reported that 87 of 154 malignant human neoplasms did not show detectable Glut-1, indicating that other Gluts may mediate glucose uptake in these tumors [16]. We therefore believe that glucose uptake in this patient may be mediated by glucose transporters other than Glut-1. Conversely, CCC showed high ^{18}F-FDG uptake and increased expression of Glut-1, whereas HK-II was not expressed (Fig. 1a–f). An earlier study mentioned that glucose-6-phosphate production depends more on the activity of HK-II than on the level of Glut-1 expression, which might be the cause of the lack of expression of HK-II in CCC [17]. The exact mechanism underlying the differential ^{18}F-FDG uptake and the expression of Glut-1 and HK-II in the tumor is still under debate. However, in our cases, the variation in the expression of Glut-1 and HK-II in HCC and CCC might be owing to the difference in origin and the different mechanisms such as glucose uptake, rate of glucose transporters, and hexokinase activity involved in the glycolytic pathway. The low sensitivity of ^{18}F-FDG PET in detecting HCC is believed to be owing to the low expression of Glut-1 and the varying activity of glucose-6-phosphate. However, in CCC the activity of glucose-6-phosphate is low, and the sensitivity of ^{18}F-FDG PET is therefore high [3]. A recent study mentioned that the mechanisms involved in glucose uptake and glycolytic mechanism appear to be different in HCC and CCC [18].

Further studies on large populations are necessary to elucidate the molecular mechanism underlying the ^{18}F-FDG uptake and expression of different glucose transporters and different hexokinase activities in HCC and CCC to facilitate a better understanding and interpretation of ^{18}F-FDG PET.

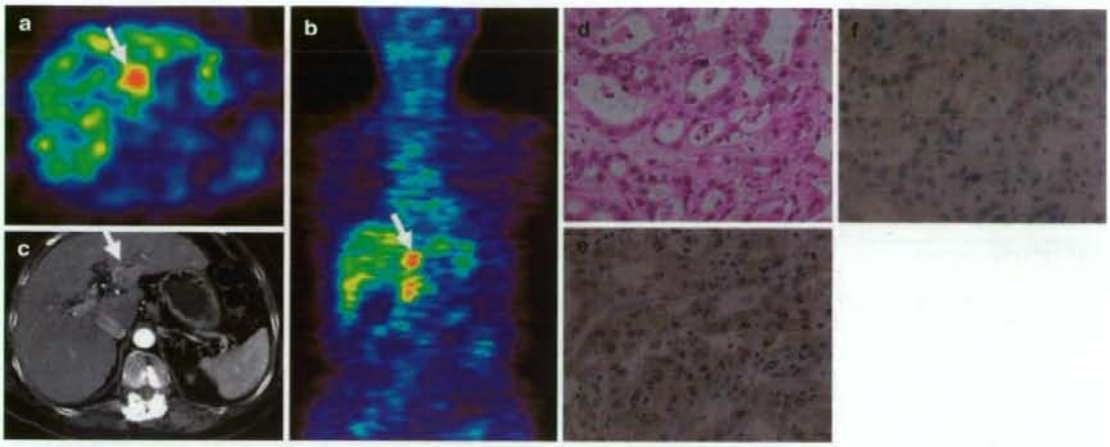

Fig. 1 ^{18}F-fluorodeoxyglucose positron emission tomography (FDG PET), corresponding computed tomography (CT) and immunohistochemistry results of glucose transporter 1 (Glut-1) and hexokinase II (HK-II) in cholangiocellular carcinoma (CCC). **a**, **b** High uptake of ^{18}F-FDG [maximal standardized uptake value (SUV) = 3.25] is seen in CCC (*arrow*). **c** Portal phase of enhanced CT shows an enhanced mass lesion at the hepatic hilum with dilation of the left intrahepatic bile duct, consistent with CCC. **d** Hematoxylin and eosin confirmed the moderately differentiated CCC. **e** Immunohistochemical staining shows strong expression of Glut-1. **f** No expression of HK-II is noted

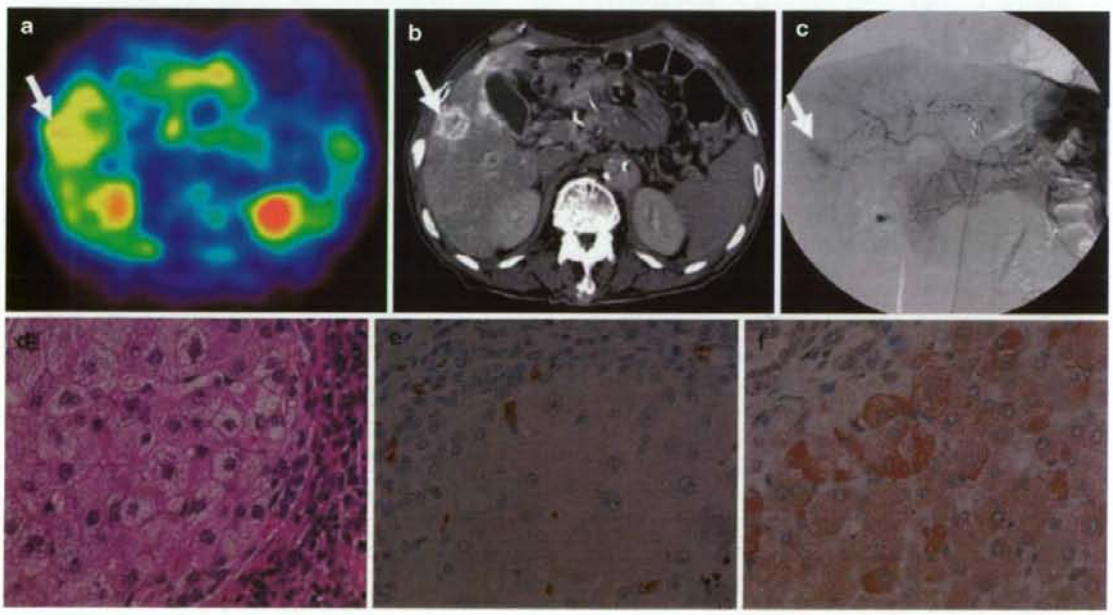

Fig. 2 ^{18}F-FDG PET, corresponding CT, angiography, and immunohistochemistry results of Glut-1 and HK-II in hepatocellular carcinoma (HCC). **a** Moderate uptake of ^{18}F-FDG (maximal SUV = 2.21) is seen in HCC located in the right hepatic lobe (*arrow*). **b** CT shows a hypervascular tumor in S5 of the liver. **c** Celiac angiography shows a tumor stain via right hepatic artery. **d** Hematoxylin and eosin confirmed the moderately differentiated HCC. **e** Immunohistochemical staining of Glut-1 shows no expression. **f** Immunohistochemical staining of HK-II shows strong expression of HK-II in the cytoplasm (original magnification, ×400)

Acknowledgments These cases were presented at the 9th Congress of the World Federation of Nuclear Medicine and Biology (WFNMB), Seoul, Korea in October 2006. We thank Masako Saito and Toshiaki Hikino of the Department of Tumor Pathology, Gunma University for their technical support. This work was supported by grants from the Ministry of Education, Culture, Sports, Science and Technology of Japan and the 21st century, Center of Excellence (COE) program of Gunma University.

References

1. Bosch FX, Ribes J, Borras J, Diaz M. Epidemiology of hepatocellular carcinoma. Clin Liver Dis 2005;9:191–211.
2. Petrowsky H, Wildbrett P, Husarik DB, Hany TF, Tam S, Jochum W, et al. Impact of integrated positron emission tomography and computed tomography on staging and management of gallbladder cancer and cholangiocarcinoma. J Hepatol 2006;45:43–50.
3. Anderson CD, Rice MH, Pinson CW, Chapman WC, Chari RS, Delbeke D. Fluorodeoxyglucose PET imaging in the evaluation of gallbladder carcinoma and cholangiocarcinoma. J Gastrointest Surg 2004;8:90–7.
4. Kim YJ, Yun M, Lee WJ, Kim KS, Lee JD. Usefulness of ^{18}F-FDG PET in intrahepatic cholangiocarcinoma. Eur J Nucl Med Mol Imaging 2003;30:1467–72.
5. Brown RS, Goodman TM, Zasadny KR, Greenson JK, Wahl RL. Expression of hexokinase II and Glut-1 in untreated human breast cancer. Nucl Med Biol 2002;29:443–53.
6. Higashi T, Saga T, Nakamoto Y, Ishimori T, Mamede MH, Wada M, et al. Relationship between retention index in dual-phase ^{18}F-FDG PET, and hexokinase-II and glucose transporter-1 expression in pancreatic cancer. J Nucl Med 2002;43:173–80.
7. Mamede M, Higashi T, Kitaichi M, Ishizu K, Ishimori T, Nakamoto Y, et al. [^{18}F]FDG uptake and PCNA, Glut-1, and hexokinase-II expressions in cancers and inflammatory lesions of the lung. Neoplasia 2005;7:369–79.
8. Kunkel M, Reichert TE, Benz P, Lehr HA, Jeong JH, Wieand S, et al. Overexpression of Glut-1 and increased glucose metabolism in tumors are associated with a poor prognosis in patients with oral squamous cell carcinoma. Cancer 2003;97:1015–24.
9. Cantuaria G, Fagotti A, Ferrandina G, Magalhaes A, Nadji M, Angioli R, et al. GLUT-1 expression in ovarian carcinoma: association with survival and response to chemotherapy. Cancer 2001;92:1144–50.
10. Kato H, Takita J, Miyazaki T, Nakajima M, Fukai Y, Masuda N, et al. Glut-1 glucose transporter expression in esophageal squamous cell carcinoma is associated with tumor aggressiveness. Anticancer Res 2002;22:2635–9.
11. Okazumi S, Isono K, Enomoto K, Kikuchi T, Ozaki M, Yamamoto H, et al. Evaluation of liver tumors using fluorine-18-fluorodeoxyglucose PET: characterization of tumor and assessment of effect of treatment. J Nucl Med 1992;33:333–9.
12. Torizuka T, Tamaki N, Inokuma T, Magata Y, Sasayama S, Yonekura Y, et al. In vivo assessment of glucose metabolism in hepatocellular carcinoma with FDG-PET. J Nucl Med 1995;36:1811–7.
13. Khan MA, Combs CS, Brunt EM, Lowe VJ, Wolverson MK, Solomon H, et al. Positron emission tomography scanning in the evaluation of hepatocellular carcinoma. J Hepatol 2000;32:792–7.
14. Miyakubo M, Oriuchi N, Tsushima Y, Higuchi T, Koyama K, Arai K, et al. Diagnosis of maxillofacial tumor with L-3-[18F]-fluoro-alpha-methyltyrosine (FMT) PET: a comparative study with FDG-PET. Ann Nucl Med 2007;21:129–35.
15. Goel A, Mathupala SP, Pedersen PL. Glucose metabolism in cancer: evidence that demethylation events play a role in activating type II hexokinase gene expression. J Biol Chem 2003;278:15333–40.
16. Younes M, Lechago LV, Somoano JR, Mosharaf M, Lechago J. Wide expression of the human erythrocyte glucose transporter Glut1 in human cancers. Cancer Res 1996;56:1164–7.
17. Aloj L, Caraco C, Jagoda E, Eckelman WC, Neumann RD. Glut-1 and hexokinase expression: relationship with 2-fluoro-2-deoxy-D-glucose uptake in A431 and T47D cells in culture. Cancer Res 1999;59:4709–14.
18. Lee JD, Yang WI, Park YN, Kim KS, Choi JS, Yun M, et al. Different glucose uptake and glycolytic mechanisms between hepatocellular carcinoma and intrahepatic mass-forming cholangiocarcinoma with increased ^{18}F-FDG uptake. J Nucl Med 2005;46:1753–9.

Radioimmunotherapy of human synovial sarcoma using a monoclonal antibody against FZD10

Chikako Fukukawa,[1,7] Hirofumi Hanaoka,[2,7] Satoshi Nagayama,[1] Tatsuhiko Tsunoda,[3] Junya Toguchida,[4] Keigo Endo,[5] Yusuke Nakamura[1] and Toyomasa Katagiri[1,6]

[1]Laboratory of Molecular Medicine, Human Genome Center, Institute of Medical Science, The University of Tokyo, Tokyo 108-8639; [2]Department of Bioimaging Information Analysis, Gunma University Graduate School of Medicine, Gunma 371-8511; [3]Laboratory for Medical Informatics, SNP Research Center, RIKEN (Institute of Physical and Chemical Research), Yokohama 230-0045; [4]Institute for Frontier Medical Sciences, Kyoto University, Kyoto 606-8507; [5]Department of Nuclear Medicine and Diagnostic Radiology, Gunma University Graduate School of Medicine, Gunma 371-8511, Japan

(Received October 11, 2007/Revised October 29, 2007/Accepted October 31, 2007/Online publication February 4, 2008)

We previously reported Frizzled homolog 10 (*FZD10*), a member of the Frizzled family, to be a promising therapeutic target for synovial sarcomas. In this report, we established a murine monoclonal antibody (MAb), namely, MAb 92-13 that had specific binding activity against native FZD10 product expressed in synovial sarcoma cell lines. Subsequent immunohistochemical analyses with the MAb 92-13 confirmed an absence or hardly detectable level of FZD10 protein in any normal human organs. We confirmed the specific binding activity of this MAb *in vivo* after injection of fluorescent-labeled MAb i.p. or i.v. into the mice carrying synovial sarcoma xenografts by the use of the *in vivo* fluorescent imaging system as well as radioisotopes. Moreover, MAb 92-13 was effectively internalized into the synovial sarcoma cells after its binding to FZD10 on the cell surface. A single i.v. injection of the Yttrium-90 (^{90}Y)-MAb 92-13 drastically suppressed tumor growth of synovial sarcoma in mice without any severe toxicity. Median time to tumor progression was 58 days for mice treated with ^{90}Y-MAb 92-13 and 9 days for mice treated with non-labeled antibody control or untreated mice (difference = 49 days; $P = 7 \times 10^{-5}$). This result indicates that MAb 92-13 could be utilized as the novel treatment modality for synovial sarcoma and other FZD10-positive tumors. (*Cancer Sci* 2008; 99: 432–440)

Monoclonal antibodies (MAb) against cancer-specific molecules have been proving useful in cancer treatment.[1] In addition to successful examples of clinical application of the humanized or chimeric antibodies such as trastuzumab,[2] rituximab[3] and bevacizumab,[4] a number of monoclonal antibodies against other molecular targets are in development and their antitumor activities being evaluated. These monoclonal antibodies are expected to provide hope to patients suffering tumors without any effective treatments.

Among soft tissue sarcomas, osteosarcoma, Ewing's sarcoma and rhabdomyosarcoma can be well managed by chemotherapy because of their sensitivity to it.[5–7] On the other hand, spindle cell sarcomas are resistant to chemo- and radiotherapy, and the patients usually have a poor prognosis. For synovial sarcoma, surgical treatment is effective for patients at an early stage, but no effective therapeutic choice is available to those at an advanced stage. Hence, development of novel therapeutic modalities is essential to improve patients' prognosis.

Genome-wide gene expression analysis in tumors provides useful information in identifying promising molecular targets for development of novel anticancer drugs and tumor markers. In our previous study, we analyzed gene-expression profiles of 47 soft-tissue sarcomas using a genome-wide cDNA microarray consisting of 23 040 genes and found that Frizzled homolog 10 (*FZD10*) was upregulated specifically in synovial sarcomas at a very high level.[8] *FZD10* gene product is reported to be a member of the Frizzled family and a putative Wnt signal receptor.[9] We also demonstrated that FZD10 expression was absent or hardly detectable in any normal organs except the placenta, suggesting that therapeutics targeting this molecule would cause no or little adverse reaction.[10] Experiments using siRNA implicated that FZD10 was significantly involved in the tumor growth of synovial sarcoma.[10] Furthermore, we generated the rabbit polyclonal antibody against an extracellular domain of FZD10, and found that this polyclonal antibody had antitumor activity with antibody-dependent cell-mediated cytotoxicity (ADCC) in a mouse xenograft model of synovial sarcoma.[10] Together, the antibody therapy against FZD10 could be expected to improve the clinical outcome of synovial sarcoma.

Here, we demonstrate generation of a murine monoclonal antibody against FZD10, MAb 92-13, by means of cell-immunization method and reveal its promising effect for clinical application.

Materials and Methods

Cell lines and tissue specimens. Cell lines derived from colon cancers (LoVo and SNU-C5), and monkey kidney cells transformed with SV40 T-antigen, COS7 cells, were purchased from were purchased from American Type Culture Collection (ATCC, Rockville, MD). YaFuSS, derived from synovial sarcoma, was kindly provided by Dr J. Toguchida (Faculty of Medicine, Kyoto University, Japan). SYO-1 was a gift from Dr A. Kawai (National Cancer Center, Japan), HS-SY-II from Dr H. Sonobe (Kochi University, Japan), Fuji from Dr S. Tanaka (Hokkaido University, Japan), and 1273/99 from Dr O. Larsson (Karolinska Institute, Sweden). All cells were cultured under their respective depositors' recommendation: Ham's F-12 nutrient mixture (Invitrogen, Carlsbad, CA, USA) for LoVo and 1273/99, RPMI-1640 (Sigma-Aldrich, St. Louis, MO, USA) for SNU-C5, Dulbecco's modified Eagle's medium (Invitrogen) for COS7, SYO-1, YaFuSS, HS-SY-II and Fuji. All cell lines were grown in monolayers in appropriate media supplemented with 10% fetal bovine serum (FBS) and 1% antibiotic/antimycotic solution, and maintained at 37°C in air containing 5% CO_2. Primary synovial sarcoma samples were obtained after informed consent, and snap-frozen in liquid nitrogen immediately after resection and stored at –80°C. All tissue samples from surgically resected synovial sarcomas were approved for our analysis by the ethics committees of the Faculty of Medicine, Kyoto University and Institute of Medical Science, University of Tokyo. Each tumor sample was fixed in 10% formalin and routinely processed for hematoxylin–eosin (HE) staining to establish a pathological diagnosis by Dr J. Toguchida.

[6]To whom correspondence should be addressed. E-mail: tkatagi@ims.u-tokyo.ac.jp
[7]These authors contributed equally to this work.

doi: 10.1111/j.1349-7006.2007.00701.x
© 2008 Japanese Cancer Association

Plasmid constructs. For construction of N-terminal HA-tagged FZD10-expression vector, we first generated a plasmid with a signal peptide sequence (1–22 residues of FZD10 protein) and a HA epitope tag. The cDNA fragment consisting of residues 1–22 was amplified by polymerase chain reaction (PCR) using PrimeSTAR HS DNA polymerase (Takara Bio, Ohtsu, Japan) with the following set of primers: 5′-AAGTCGACGCCAGCA-TGCAGCGCCCG-3′ and 5′-AACTCGAGGCTGATGGCGGC-GCACGAG-3′ (underlines indicate restriction enzyme sites). To generate the HA epitope tag, the following set of oligonucleotides, 5′-GCATGTCGACTACCCATACGATGTTCCAGATTACGCT CTCGAGGCAT-3′ and 5′-ATGCCTCGAGAGCGTAATCTGG-AACATCGTATGGGTAGTCGACATGC-3′ (underlines indicate restriction enzyme sites) were mixed, and denatured at 94°C for 3 min and gradually cooled down to 37°C (0.1°C/s slope) for annealing. Next, to amplify the cDNA fragment consisting of residues 23–581 of FZD10, we performed PCR using the following primers: 5′-AAGTCGACTCCATGGACATGGAGC-GCCC-3′ and 5′-AACTCGAGTCACACGCAGGTGGGCGACT-3′ (underlines indicate restriction enzyme sites). Each PCR fragment was digested with *Sal*I and *Xho*I and ligated into a pCAGGS/neo vector, sequentially (pCAGGS/neo-HA-FZD10; FZD10-2). Construction of pCAGGS/neo-FZD10-myc/His (FZD10-myc/His) was conducted according to our previous report.[10] DNA sequences of all constructs were confirmed by DNA sequencing (ABI3700; PE Applied Biosystems, Foster, CA, USA).

Semi-quantitative reverse transcription (RT)-PCR. Total RNA were extracted from each of the cell lines and primary tumor samples using TRIzol reagent (Invitrogen). The extracted RNA were treated for 30 min at room temperature with 30 units of DNase I (Roche, Basel, Switzerland) in the presence of 1 unit of RNase inhibitor (Toyobo, Osaka, Japan) to remove any contaminating genomic DNA. After inactivation at 70°C for 10 min, 3-μg aliquots of each total RNA were reversely transcribed for single-stranded cDNA using oligo $(dT)_{12-18}$ primer and Superscript II (Invitrogen) at 42°C for 60 min. We prepared appropriate dilutions of each single-stranded cDNA for subsequent PCR by monitoring β2-microglobulin (*β2MG*) as a quantitative control. PCR amplification was performed using Ex-taq polymerase (Takara Bio) and the cDNA as templates with the primers: 5′-TATCGGGCTCTTCTCTGTGC-3′ and 5′-GACTGGGCAGGG-ATCTCATA-3′ for *FZD10*; 5′-TTAGCTGTGCTCGCGCTACT-3′ and 5′-TCACATGGTT CACACGGCAG-3′ for *β2MG*. PCR were optimized for the number of cycles to ensure product intensity within the logarithmic phase of amplification. The PCR conditions were 94°C for 30 s, 58°C for 30 s and 72°C for 30 s for 21 cycles (for *β2MG*) and 28 cycles for *FZD10*, respectively. The PCR products were resolved by electrophoresis on 2.0% ethidium bromide-stained agarose gels, and band intensity was quantified with the use of NIH Image analysis software (http://rsb.info.nih.gov/nih-image/).

Generation of murine anti-FZD10 monoclonal antibody (MAb) with cell immunization. Murine anti-FZD10 MAbs were generated by immunizing four-week-old female BALB/c mice with COS-7 cells transfected with pCAGGS/neo-FZD10-myc/His for three times every 3 days (Medical and Biological Laboratories, Nagoya, Japan). Lymph node cells from the immunized mice were harvested and fused with the myeloma cell line. The hybridomas were subcloned and assayed by cell ELISA for the ability to secrete immunoglobulin that binds to the extracellular domain of FZDIO. Fifty microliters of cells in phosphate-buffered saline (PBS) (2.5×10^6 cells) were subcloned and assayed by cell enzyme-linked immunosorbent assay (ELISA) for the ability to secrete immunoglobulin that binds to the extracellular domain of FZD10. For cell ELISA, COS-7 cells expressing FZD10-myc/His were seeded into 96-well ELISA plates (Nalgen Nunc International, Naperville, IL, USA). Subsequently, 50 μL of the culture supernatants obtained from hybridomas were added to the plate and incubated for 30 min at room temperature. After washing the cells with PBS (–), goat antimouse immunoglobulin (Ig)G-POD (Medical and Biological Laboratories) was added at 1:10 000 dilution, incubated for 30 min at room temperature. Bound antibodies were detected at $OD_{450-620}$nm by using Ultramark Microplate Reader (Bio-Rad, Hercules, CA, USA). Positive clones were further analyzed for specific binding activity. The MAb were affinity purified on protein G-sepharose for further characterization.

Cell transfection. For confirmation of binding-specificity of MAb 92-13, SNU-C5 cell was transiently transfected with mock vector (pCAGGS-neo) or pCAGGS/neo-FZD10-myc/His construct using FuGENE 6 transfection regent (Roche) according to manufacturer's protocol. For establishment of stably overexpressing-FZD10 cells, HA-tagged FZD10-expression vector (pCAGGS/neo-HA-FZD10) or mock vector (pCAGGS-neo) was transfected into 1273/99 synovial sarcoma cells, in which undetectable expression of FZD10 was observed, using Lipofectamine2000 (Invitrogen) according to manufacturer's protocol. Transfected cells were incubated in the culture medium containing 0.2 mg/mL neomycin (geneticin; Invitrogen). Three weeks later, 20 individual colonies were selected by limiting dilution and screened for HA-FZD10 stably overexpressing clones. The expression level of HA-FZD10 was detected in each clone by western blot and immunocytochemical staining analyses using anti-HA monoclonal antibody (Roche).

Immunohistochemical staining analyses. For immunohistochemical staining analysis, 4-μm sections of paraffin-embedded normal adult human tissues (lung, heart, liver, kidney, colon and placenta) (BioChain, Hayward, CA, USA) and surgical synovial sarcoma specimens were deparaffinized and processed for antigen retrieval in Target Retrieval Solution (pH 9) (DAKO Cytomation, Carpinteria, CA, USA) at 125°C for 30 s. After treatment with peroxidase blocking reagent (DAKO Cytomation) for 10 min, followed by treatment with protein blocking serum-free (DAKO Cytomation) for 30 min, slides were incubated with 10 μg/mL MAb 92-13. Subsequently, ENVISION Polymer Reagent (DAKO Cytomation) was added and visualized with peroxidase substrate (3,3′-diaminobenzidine tetrahydrochloride; Sigma-Aldrich).

Labeling antibodies with radionuclides. Iodine-125 (^{125}I)-labeled MAb 92-13 was prepared according to standard protocols of chloramine-T method.[11] 740 kBq/2 μL of Na ^{125}I (GE Healthcare, Buckinghamshire, UK) was added to 10 μg MAb 92-13 in 100 μL of 0.3-M sodium phosphate buffer solution. One-microgram of chloramine-T in 3 μL of 0.3-M sodium phosphate buffer was further added and incubated for 5 min at room temperature. Labeled antibody was purified using Biospin column 6 (Bio-Rad) according to manufacture's instructions. For labeling MAb with Indium-111 (^{111}In), 1 μg of MAb in 100 μL of 50-mM borate buffer (pH 8.5) was conjugated to isothiocyanatobenzyldiethylenetriaminepentaacetic acid (SCN-BZ-DTPA; Macrocyclics, Dallas, TX, USA) in dimethylformamide at molar ratio 1:3. After incubation at 37°C for 20 h, MAb conjugates were purified using Biospin Column 6 (Bio-Rad). Forty microliters of $^{111}InCl_3$ (Nihon Medi-Physics, Hyogo, Japan) was incubated in 60 μL of 0.25-M acetic acid solution (pH 5.5) and incorporated into 10 μg/mL of MAb-DTPA conjugates for 1 h at room temperature. Labeled antibody was purified using Biospin Column 6 (Bio-Rad) according to manufacture's instructions. For labeling MAb with Yttrium-90 (^{90}Y), 600 μL of ^{90}Y solution (Chiyoda Technol, Tokyo, Japan) was incubated with 400 μL of 0.25-M acetic acid solution (pH 5.5) for 5 min at room temperature, followed by incubation with 300 μg of MAb-DTPA conjugates for 1 h at 45°C. It was confirmed that there was no degradation of MAb during incubation. Labeled antibody was purified using PD-10 column (GE Healthcare) according to manufacture's instructions.

Characterization of binding activity of MAb 92-13. We applied two methods for evaluation of the binding affinity of mouse-monoclonal; flow cytometric analysis with fluorescent dyes and radioactive measurement using ^{125}I. For flow cytometric analysis

© 2008 Japanese Cancer Association

with indirect fluorescence, suspensions of 5×10^5 cells were incubated with 10 μg/mL of MAb 92-13 or non-immunized mouse IgG (Beckman Coulter, Fullerton, CA, USA) for 30 min at 4°C. After washing with PBS (–), 2 μg Alexa Fluor 488-fluorescent goat antimouse IgG or Alexa Fluor 488-goat antihuman IgG (Molecular Probes) were added, and the cell suspension was incubated for 30 min at 4°C for FACScan analysis (Becton Dickinson, Franklin Lakes, NJ, USA).

To evaluate the nonspecific binding activity of MAb 92-13 against normal blood cells, ^{125}I-labeled MAb 92-13 (5 ng antibody) was incubated with 100 μL of each of three healthy volunteers' fresh blood (donors A, B and C), and was further added with a non-labeled identical MAb 92-13. After incubation for 1 h at room temperature, the cell suspension was centrifuged at 1000*g*. The supernatant was removed and the radioactivity of each cell pellet was measured.

Immunoprecipitation (IP): western blot analysis. Cells were lyzed with lysis buffer (50 mM Tris-HCl, 0.5% Igepal, 0.5% TritonX-100, 2% glycerol, 150 mM NaCl, 1 mM NaF, 1 mM sodium orthovanadate, pH 7.4) including 0.2% protease inhibitor cocktail III (Calbiochem, San Diego, CA, USA). After homogenization, the cell lysates were incubated on ice for 30 min and centrifuged at 17 000*g* for 15 min to separate only supernatant from cell debris. Then, the lysates were subjected to immunoprecipitation. The amount of total protein was estimated by protein assay kit (Bio-Rad). One milligram protein was mixed with protein G-sepharose and 1 μg antibodies as indicated. The mixtures were incubated for 1 h at 4°C and the precipitated beads were washed with lysis buffer five times. The bound proteins were eluted with sodium dodecylsulfate (SDS)-sample buffer and subjected to SDS-polyacrylamide gel electrophoresis. After electrophoresis, the proteins were blotted onto nitrocellulose membrane (GE Healthcare). After blocking with 4% BlockAce blocking solution (Dainippon Pharmaceutical, Osaka, Japan), membranes were incubated with the primary antibody, HA (1:3000 dilution; Anti-HA High Affinity, clone 3F10; Roche). Finally, the membrane was incubated with HRP conjugated secondary antibody (1:30 000 dilution; Santa Cruz Biotechnology, Santa Cruz, CA, USA), and protein bands were visualized by ECL detection reagent (GE Healthcare).

Tumor xenograft models. Animal care and treatment was performed in accordance with the guidelines of animal use and animal committee of the University of Tokyo. The above committee approved all procedures. BALB/cA Jcl-nu mice (female, 6 weeks old) were purchased from CLEA Japan (Tokyo, Japan). Mice were maintained under specific pathogen-free conditions and provided with sterile food and water ad libitum. BALB/cA Jcl-nu mice were injected s.c. with SYO-1 tumor cells (5×10^6 cells) or LoVo tumor cells (1×10^7 cells), in 0.1 mL PBS, in the flanks, respectively. For biodistribution studies, mice with fully established tumors (0.5 cm^3) were given 10 kBq (0.5–1 μg) of ^{111}In-labeled MAb 92-13 via tail vain. Animals were killed 1, 24 and 48 h after administration, and weight and radioactivity of each tissue were measured. The distribution was expressed as percentage of injected dose/g of tissue for all samples. To examine the specificity of radiolabeled MAb 92-13 *in vivo*, we examined the biodistribution of ^{111}In-labeled MAb 92-13 in SYO-1-tumor xenografts pretreated with non-labeled identical antibody. SYO-1-tumor bearing BALB/c nude mice were injected with 400 μg of non-labeled MAb 92-13 20 min prior to the injection of 10 kBq of ^{111}In-labeled MAb 92-13. Both injections were performed i.v. They were compared with the mice that were injected with ^{111}In-labeled MAb 92-13 without pretreatment of non-labeled identical antibody. The normal organs and tumors were dissected at 48 h after the injection, and the radioactivities were measured. For optical imaging of biodistribution, the mice were subjected to the imaging study when tumors were fully established (0.2 cm^3). *In vivo* fluorescence imaging was performed with the IVIS Imaging System 100 series (Xenogen, Alameda, CA, USA). Labeling of MAb 92-13 with Alexa-Fluoro 647 was carried out using a Alexa647 Monoclonal Antibody Labeling Kit (Molecular Probes) according to manufacturer's instructions. The Alexa647 reactive dye has a succinimidylester moiety that reacts with primary amines of proteins, and resulting MAb-dye conjugates were purified by size exclusion column. An optimized Cy5.5 filter was used to acquire Alexa647-MAb 92-13 fluorescence *in vivo*. Tumor-bearing mice were injected 20 μg Alexa647-labeled MAb 92-13 i.p. and subjected to fluorescent imaging at various time points. The mice were fed with food not containing alfalfa (CLEA Japan) for 4 days in prior to injecting MAb 92-13 in order to reduce the background fluorescence. When acquiring images, mice were anesthetized with 2% of isoflurane (Abbott Laboratories, Abbott Park, IL, USA) and placed in the IVIS system. The mice were killed 5 days after injection of MAb 92-13, the synovial sarcoma tumor and major mouse organs (liver, spleen, kidney, pancreas and colon) were dissected, and fluorescence images of each organ were obtained.

For therapy studies, SYO-1 tumors were grown in BALB/cA Jcl-nu mice in the same way. The diameters of the tumors were measured by calipers and the tumor volumes were determined using the following formula: $0.5 \times (\text{larger diameter}) \times (\text{smaller diameter})^2$ as described previously.[10] When the tumors were fully established (0.016–1.3 cm^3), animals were randomly assigned to treatment groups so that the mean tumor volume of each treatment group was approximately 0.56 cm^3. Those mice received i.v. injections of the 100 μCi of ^{90}Y-MAb 92-13, non-labeled MAb 92-13 as a control. Mice were weighed and tumor diameters were recorded.

Internalization analysis of MAb 92-13 by confocal microscopy and flow cytometric (FACS) analyses. For microscopic analysis, cells were plated into 8-well chamber slides (Nalgen Nunc International) at density of 5×10^4 cells/well. Cells were incubated with 30 μg/mL MAb 92-13 for 3 h at 37°C in an air chamber containing 5% CO_2. The antibodies bound to the cell surface were removed with acid stripping buffer (0.1 M glycine, 500 mM NaCl, pH 2.5) at 4°C for 10 min, and neutralized with 500 mM Tris-Cl (pH 7.5). Cells were then fixed with 3.7% formaldehyde for 15 min at room temperature, and permeabilized by exposure to 0.2% TritonX-100 for 10 min, followed by blocking with 3% bovine serum albumin (BSA) for 1 h at room temperature. To detect the MAb 92-13 internalized into the cells, cells were incubated with Alexa Fluor488 goat anti rat IgG (H + L; 1:700 dilution) for 1 h at room temperature. The slides were mounted with DAPI (Vectashield, Vector Laboratories, Burlingame, CA, USA) and analyzed under Leica TCS SP1 confocal optics (Leica). For FACS analysis, SYO-1 (5×10^6) cells were incubated in 100 μL of Dulbecco's modified Eagle medium (DMEM) containing 10% FBS with 2 μg Alexa488-labeled MAb 92-13 or PBS (pH 7.2) as a control. The labeled-MAb 92-13 bound to FZD10 on the surface of cells at 4°C for 1 h. Subsequently, cells were incubated at 37°C for 3 h to allow the internalization of labeled-antibodies. To determine the amount of internalized anti-FZD10 MAb into the cells, the labeled-antibodies bound to the cell surface were removed with acidic PBS (pH 2.0) at 4°C for 10 min, and then cells were washed three times with PBS (pH 7.2), and subjected to FACS analysis. As a control, cells were kept at 4°C after stripping of the labeled antibodies that bound to the cell surface. For measurement of fully cell-bound antibody as a positive control, cells were not treated with acidic PBS (pH 2.0) after the treatment of labeled antibodies.

Statistical analysis. Data points represent the means along with 95% confidence intervals (CI) of multiple independent experiments. The two-sample Student's *t*-test with Welch's correction was used for two-group comparisons of tumor volumes (^{90}Y-MAb 92-13 vs non-labeled MAb 92-13 and ^{90}Y-MAb 92-13 vs ^{90}Y-α-CD20) in *in vivo* therapeutic experiments. Time to tumor

doi: 10.1111/j.1349-7006.2007.00701.x
© 2008 Japanese Cancer Association

progression was defined a priori as the time when tumor volume had increased 2.5 times from the baseline value for each mouse according to a previous report.[12] The Kaplan–Meier method was used to determine the median time to tumor progression. All *P*-values for the xenograft studies were based on comparisons of time to tumor progression among groups by use of the log–rank test. All statistical tests were two-sided, and *P*-values less than 0.05 were considered to be statistically significant.

Results

Generation of anti-FZD10 MAb 92-13. We attempted to generate an anti-FZD10 antibody for treatment of synovial sarcoma (see Materials and Methods). Balb/c mice were immunized with living COS-7 cells transiently transfected with FZD10-myc/His construct, and hybridomas were obtained. Among hosts of these hybridoma clones, one clone, 92-13, was selected as a candidate to produce an antibody against FZD10 by cell ELISA assay. The MAb 92-13 was determined to produce the IgG2a isotype by means of the IsoStrip Mouse Monoclonal antibody isotyping kit (Roche). To investigate the cell-binding affinity of MAb 92-13, we performed flow cytometry (FACS) experiments. MAb 92-13 bound to cell surfaces of four FZD10-overexpressing synovial sarcoma cell lines, SYO-1, YaFuSS, HS-SY-II and Fuji, but did not bind to two cell lines, 1273/99 and LoVo, in which no transcript of FZD10 was detected (Fig. 1a,b). We found a significant correlation of relative mean fluorescent intensities (MFI) of MAb 92-13 with the expression levels of FZD10. In addition, MAb 92-13 also bound to the SNU-C5 cells transfected with an FZD10-myc/His construct, while no binding was detected with SNU-C5 cells transfected with an empty vector (Fig. 1c), further supporting the specific binding affinity of MAb 92-13 to FZD10. We further confirmed that this antibody could specifically immunoprecipitate FZD10 protein in HA-tagged FZD10-overexpressing cells (FZD10-2), but not in mock-transformant cells (Mock1; Fig. 1d), suggesting that MAb 92-13 has an ability to specifically recognize the native FZD10.

We also performed immunohistochemical staining analysis using MAb 92-13 in order to confirm FZD10 expression at protein level in human normal tissues and synovial sarcoma tissues (Fig. 2a,b). In concordance with the transcript level,[10] we detected a high level of FZD10 protein in two synovial sarcoma specimens examined, and an absence or a hardly detectable level of FZD10 protein in normal human colon, heart, lung, liver and kidney except placenta tissue (Fig. 2c–h).

***In vivo* distributions of anti-FZD10 MAb in mice xenograft model.** *In vivo* distribution of MAb 92-13 was examined by means of two independent methods, fluorescent imaging and radionuclide activity, using mice in which synovial sarcoma xenograft was implanted. For *in vivo* imaging using fluorescence, 20 μg Alexa647-labeled MAb 92-13 was injected i.p. into the SYO-1-bearing mice, and distribution of the MAb was visualized using

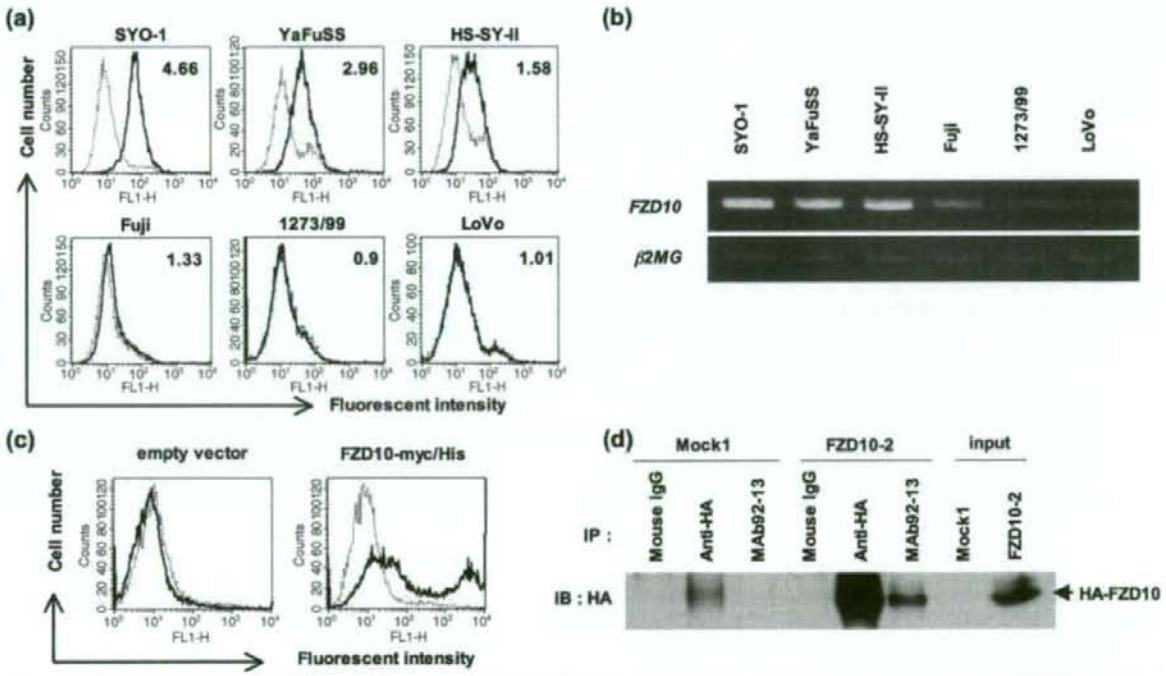

Fig. 1. Characterization of binding specificity for anti-FZD10 monoclonal antibody (MAb) 92-13. (a) Flow cytometric analysis of MAb 92-13 using five synovial sarcoma cell lines (SYO-1, YaFuSS, HS-SY-II, Fuji and 1273/99) and one colon cancer cell line (LoVo). Solid lines show the fluorescent intensity detected by MAb 92-13; broken lines depict the fluorescent intensities of cells incubated with non-immunized mouse immunoglobulin (Ig)G as a negative control. The number within each panel indicates mean fluorescent intensities (MFI) of MAb 92-13 against each cell line. (b) Semiquantitative reverse transcription polymerase chain reaction (RT-PCR) of *FZD10* transcript in the same cell lines as shown in (a). *β2MG* served as an internal control. (c) Flow cytometric analysis of MAb 92-13 against exogenous FZD10. Colon cancer cell line, SNU-C5, was transfected with pCAGGS/neo empty vector (left panel) or pCAGGS-FZD10-myc/His (right panel), and analyzed at 48 h after the transfection. Solid lines show the fluorescent intensity detected by MAb 92-13; broken lines depict the fluorescent intensities of cells incubated with non-immunized mouse IgG as a negative control. (d) Specificity of MAb 92-13. Immunoprecipitate (IP)-western blot analysis of FZD10 protein in 1273/99 cells in which HA-tagged FZD10 was stably expressed (FZD10-2) or those transfected with mock vector (Mock1) was performed. Mouse IgG is control for IP experiments.

© 2008 Japanese Cancer Association

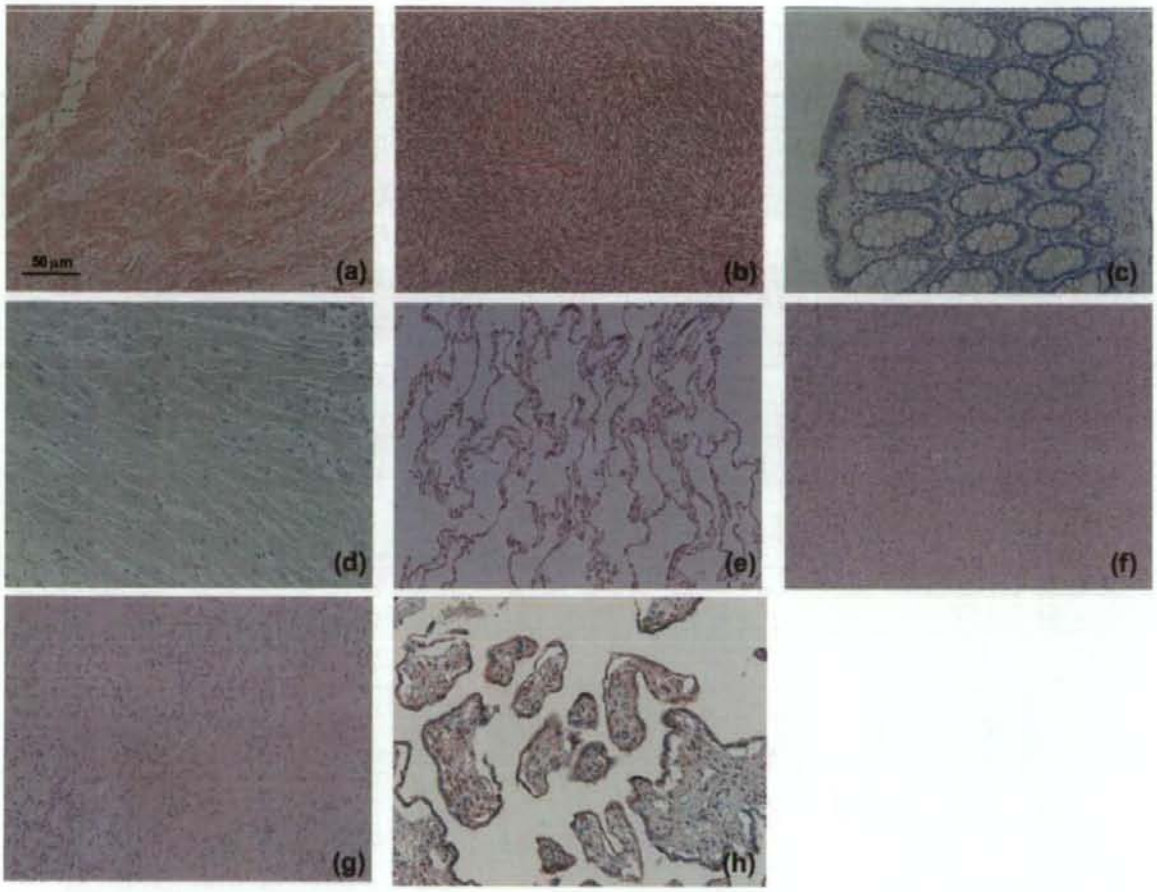

Fig. 2. Immunohistochemical staining analyses of synovial sarcoma and normal human tissue sections using MAb 92-13; (a,b) synovial sarcoma tissue sections (c) colon, (d) heart, (e) lung, (f) liver, (g) kidney and (h) placenta. Original magnification ×100. Bar, 50 μm.

the IVIS system (see Materials and Methods). Obvious accumulation of the fluorescent signal was detected at the location of tumor 24 h after the injection (Fig. 3a, upper panels). The fluorescent signal reached maximum level at approximately 48 h, and could be detectable at 96 h after the injection. Then, we killed these mice at a 120-h time point, and measured the fluorescence intensity in the tumor as well as some normal organs (liver, spleen, kidney, pancreas and colon). A very strong fluorescence signal was observed in the dissected tumor, whereas no fluorescence signal was detected in any normal organs examined (Fig. 3a, lower panels). As a control, we also generated xenografts of the FZD10-negative LoVo cell line in nude mice and performed fluorescent imaging analysis after injection of Alexa647-labeled MAb 92-13. In these mice, the fluorescent signal was detected neither at the location of the tumor (Fig. 3b, upper panels), in the dissected tumor nor in any other organs examined (liver, spleen, kidney, pancreas and colon) (Fig. 3b, lower panels).

We further confirmed accumulation of MAb 92-13 using Indium-111 (^{111}In) label; the radioactivity in the blood dropped from 35% of the injected-dose per gram (%ID/g) at 1 h to 12% at 48 h after the injection (Fig. 3c). Radioactivities in blood, liver, kidney, intestine, spleen, pancreas, lung, heart, stomach and muscle remained constantly or decreased gradually throughout the observation, whereas radioactivity in the tumors accumulated throughout the experiment from 2%ID/g at 1 h after the injection to 11%ID/g after 48 h. On the other hand, ^{111}In-labeled MAb 92-13 (^{111}In-MAb 92-13) did not accumulate to tumor in LoVo-tumor bearing mice (Fig. 3d). Furthermore, when SYO-1-bearing mice were injected with an excess amount of non-labeled MAb 92-13 i.v. prior to injection of ^{111}In-MAb 92-13, accumulation of radiolabeled antibody to tumor was completely blocked (Appendix I, Fig. S1). Because we previously reported that LoVo cells express all molecules of the FZD family (FZD1-FZD9) except FZD10,[10] ^{111}In-labeled MAb 92-13 specifically bound to the FZD10 molecule on the cell surface of synovial sarcoma *in vivo*.

Internalization of MAb 92-13 into synovial sarcoma cells. As described above, the observation by *in vivo* imaging IVIS system indicated accumulation of MAb 92-13 at the tumor region at 5 days after the injection. Hence, we examined a level of internalization of MAb 92-13 into the cells by confocal microscopy using Alexa488-labeled goat antimouse IgG antibody. By the method described above, we observed effective incorporation of MAb 92-13 into the cytosol of SYO-1 and YaFuSS cells at 3 h

doi: 10.1111/j.1349-7006.2007.00701.x
© 2008 Japanese Cancer Association

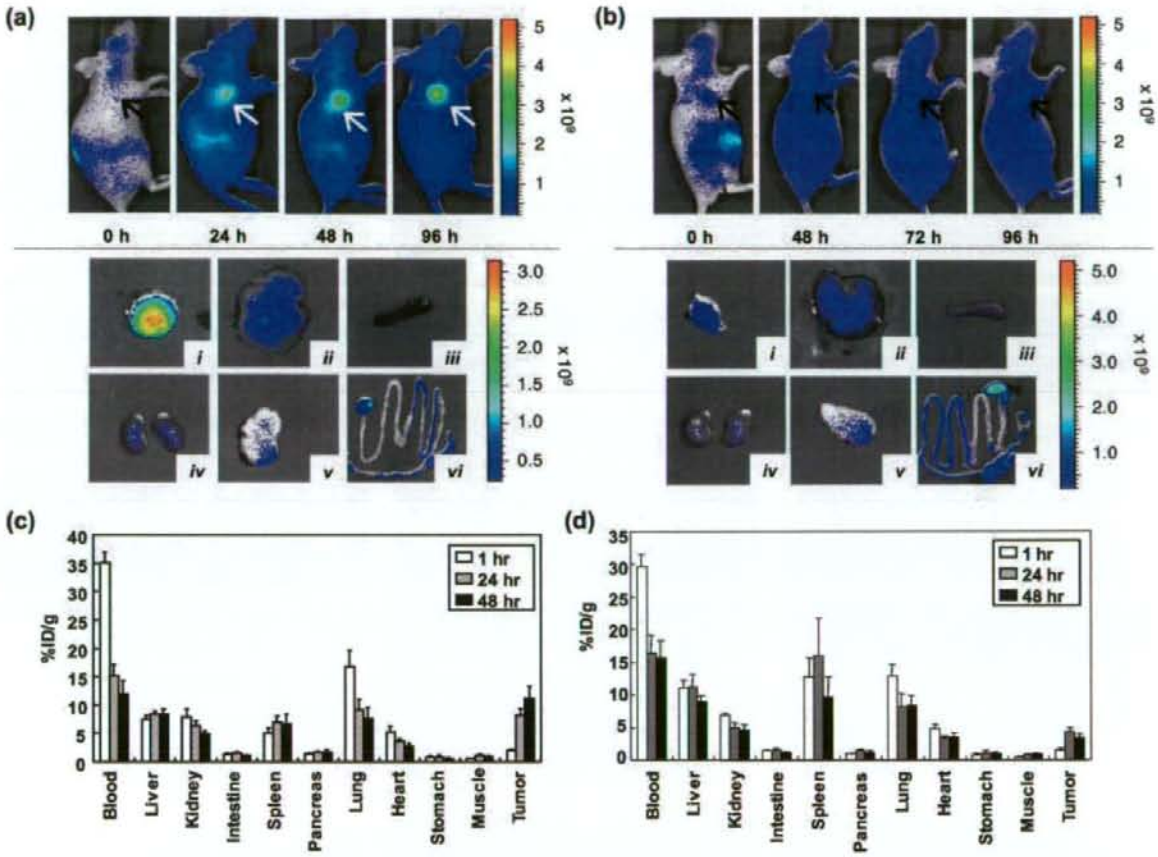

Fig. 3. Biodistribution of MAb 92-13 *in vivo*. (a, upper panels) *In vivo* fluorescence imaging of SYO-1-tumor bearing mice after injection of Alexa647-labeled MAb 92-13. Fluorescence-labeled antibody was administered at a dose of 20 μg per mouse i.p. All fluorescence images were acquired with a 60-s exposure time (f/stop = 2) immediately after the injection (0 h) and at 24, 48 and 96 h after the injection. The arrows indicate the position of the tumor. Fluorescence signal from Alexa647 was pseudo-colored according to the color bar indicated on right. (Lower panels). Representative images of dissected organs and tumors from mice shown in upper panels; (i) SYO-1 tumor; (ii) liver; (iii) spleen; (iv) kidney; (v) pancreas; and (vi) colon. (b, Upper panels) *In vivo* fluorescence imaging of LoVo-tumor bearing mice after the injection of Alexa647-labeled MAb 92-13. Images were obtained at 0, 48, 72 and 96 h after the injection of fluorescent-labeled antibody as described in upper panels. (Lower panels) Representative images of dissected organs and tumors from mice shown in upper panels; (i) LoVo tumor; (ii) liver; (iii) spleen; (iv) kidney; (v) pancreas; and (vi) colon. (c) Biodistribution of ^{111}In-labeled MAb 92-13 in SYO-1 xenografts. Ten kBq of ^{111}In-labeled 92-13 was injected i.v. into SYO-1-tumor bearing BALB/c nude mice. The normal organs and tumor were dissected at 1 h (open bar), 24 h (hatched bar) and 48 h (closed bar) after the injection, and the radioactivities were measured. The data shown are the representative data in two independent experiments. (d) Biodistribution of ^{111}In-labeled MAb 92-13 LoVo in tumor xenografts. Ten kBq of ^{111}In-labeled MAb 92-13 was injected i.v. into LoVo-tumor bearing BALB/c nude mice. The normal organs and tumors were dissected at 1 h (open bar), 24 h (hatched bar) and 48 h (closed bar) after the injection, and the radioactivities were measured. The data shown are the representative data in two independent experiments.

after the incubation of the MAb 92-13 (Fig. 4ai,ii) compared to PBS treatment as a control (Fig. 4aiv,v). On the other hand, its fluorescence signal was hardly detectable in LoVo cells in which the FZD10 expression was absent (Fig. 4aiii,vi), indicating the effective internalization of the MAb 92-13 into FZD10-overexpressing synovial sarcoma cells. Furthermore, we performed FACS analysis to validate the internalization of MAb92-13. We also observed the incorporation of this antibody into the SYO-1 cells at 3 h after the incubation of the MAb 92-13 according to the method described above (Fig. 4b). Taken together, our results suggest that MAb 92-13 was internalized into the cell in an FZD10-specific manner.

Effect of ^{90}Y-labeled MAb 92-13 on tumor growth. We then applied the radioimmunotherapy using ^{90}Y-labeled MAb 92-13 (^{90}Y-MAb 92-13) for treatment of synovial sarcoma tumors. Balb/c nude mice were injected s.c. in their flanks with SYO-1 cells. When tumors were fully established (0.016–1.3 cm^3; mean volume = 0.56 cm^3/group), mice were administrated i.v. with 100 μCi of ^{90}Y-MAb 92-13, 100 μCi of ^{90}Y-α-CD20, non-labeled MAb 92-13, or were not treated. Tumors in mice treated with non-labeled MAb 92-13 grew very rapidly and exceeded 3 cm^3 in 12 days and those of untreated mice became more than 3 cm^3 at day 16 (Fig. 5a). The sizes of tumors in mice treated with ^{90}Y-α-CD20 were transiently reduced in the first 14 days after the treatment, but the tumors regrew very rapidly and exceeded 3 cm^3 in 33 days. On the other hand, in all of the mice that received 100 μCi of ^{90}Y-MAb 92-13, tumor volumes were markedly reduced immediately after the treatment. The mean

© 2008 Japanese Cancer Association

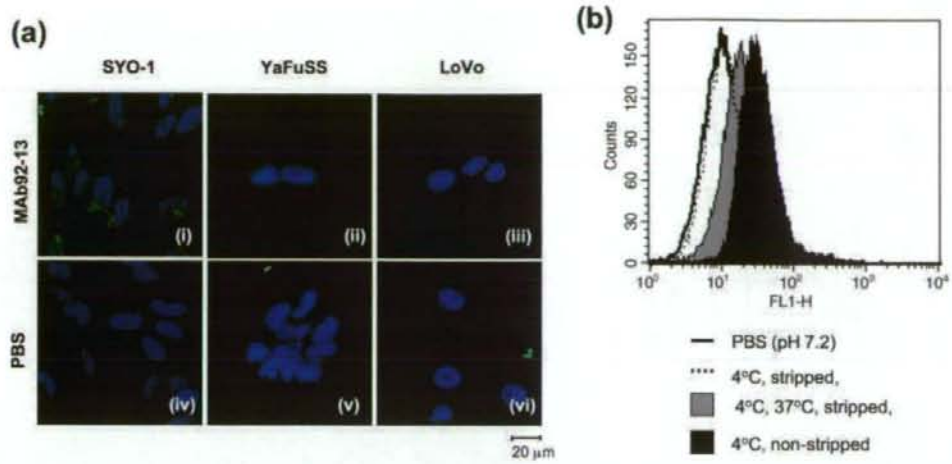

Fig. 4. Internalization of MAb 92-13 into FZD10-expressing cells. (a) Internalized antibody was assessed by confocal microscopy. Cells were treated with 30 μg/mL of MAb 92-13 (i–iii) or phosphate-buffered saline (PBS) (iv–vi) for 3 h at 37°C. Antibodies bound to the cell surface were acid-stripped with 0.1 M glycine buffer (pH 2.5). Cells were fixed, permeabilized and then blocked with 3% bovine serum albumin (BSA). Intracellular antibodies were detected with goat antimouse IgG-Alexa488 and nucleus was stained with DAPI. (i,iv) SYO-1; (ii,v) YaFuSS; (iii,vi) LoVo. Bar, 20 μm. (b) Detection of the internalized antibody by FACS analysis. The Alexa488 labeled-MAb92-13 antibodies were bound to the surface of SYO-1 cells at 4°C, followed by incubation at either 4°C (broken line histgram) or 37°C (gray histgram and black histgram) for 3 h. Cells were also incubated with PBS (pH 7.2) as a control (solid line histgram). To remove the antibodies that bound to the cell surface, cells were treated with (broken line histgram and gray histgram) or without acidic-PBS (black histgram).

tumor volume of ^{90}Y-MAb 92-13-treated mice was decreased to approximately 0.1 cm^3 at day 9 after the injection. Median time to tumor progression, as defined by tumors reaching 2.5-times baseline size in accordance with a previous report,[12] was 58 days for mice injected with ^{90}Y-MAb 92-13, 23 days for mice injected with ^{90}Y-α-CD20 and 9 days for mice injected with non-labeled 92-13 or left untreated (^{90}Y-MAb 92-13 vs ^{90}Y-α-CD20; $P = 2 \times 10^{-5}$, ^{90}Y-MAb 92-13 vs non-labeled MAb 92-13; $P = 7 \times 10^{-5}$, ^{90}Y-MAb 92-13 vs no treatment; $P = 7 \times 10^{-5}$) (Fig. 5a). The tumors in seven of the 11 mice were less than 0.02 cm^3 at day 33. However, the tumor volume in seven of the 11 mice increased after day 33. Importantly, in four mice, regrowth of the tumors was not observed even at day 54 after the treatment (Fig. 5b). The mice that received ^{90}Y-MAb 92-13 and ^{90}Y-α-CD20 showed temporary decrease of the bodyweight (10–15%, Appendix I, Fig. S2), but they recovered within 1 week, and no visible toxic sign was observed until 30 days after injection (Fig. 5c). Our results indicate that a single injection of ^{90}Y-MAb 92-13 has specific and strong antitumor effect against synovial sarcoma with FZD10 expression.

Discussion

We previously reported that FZD10, a member of the Frizzled family, was significantly transactivated in synovial sarcoma, but not expressed in normal human organs except placenta,[8,10] and involved in cancer cell growth or survival by RNAi experiments.[10] Furthermore, because we demonstrated that anti-FZD10 polyclonal antibody showed antitumor activity with ADCC *in vitro* and *in vivo*,[10] we have been attempting to generate a murine monoclonal antibody against FZD10 for antibody-based synovial sarcoma therapy. Due to formation of homo-oligomerization of FZD10 as described previously,[10] it had been very difficult to generate specific monoclonal antibodies against FZD10. After failure of multiple attempts to generate anti-FZD10 monoclonal antibodies that could recognize a native form of FZD10 by the use of full-length or partial recombinant FZD10 proteins encoding the N-terminal extracellular region, we finally attempted immunize Balb/c mice by injection of living COS-7 cells in which FZD10 was exogenously introduced and overexpressed. We successfully obtained a clone of hybridoma, namely 92-13 (MAb 92-13), producing specific a murine monoclonal antibody against FZD10. To investigate the cross-reactivity of MAb 92-13 with other members of the FZD family, we demonstrated that MAb 92-13 did not bind to cell surfaces of LoVo and SNU-C5, colon cancer cell lines (Fig. 1a,c), in which all known members of the FZD family except FZD10 were expressed as described previously,[10] strongly supporting the specific binding of MAb 92-13 FZD10, but not to other FZD family members.

When antibodies are applied for cancer therapy, cross-reaction of the antibody to normal organs or blood cells there is a concern that they will cause severe adverse reactions. To investigate the *in vivo* distribution of MAb 92-13, we applied two methods; one based on the radionuclide modalities using ^{111}In-labeled antibody, and the other based on the fluorescence imaging using near-infrared-labeled antibodies. Near-infrared fluorescence is now widely used in the *in vivo* imaging for diagnostic purpose because the light of this wavelength penetrates living tissue efficiently.[13] The results obtained by two approaches were very concordant and indicated that MAb 92-13 bound and accumulated to SYO-1 tumor cells, but not to any other tissues. Moreover, we confirmed that MAb 92-13 has no immunoreactivity against normal human blood cells (Appendix I, Fig. S3), strongly implying clinical applicability of this antibody with a very minimum risk of adverse effects to patients. In addition, our *in vitro* experiments using confocal microscopy reveled that MAb 92-13 was internalized into the cell in an FZD10-specific manner. Recently, because it has been reported that Frizzled 4, a member of FZD family, was internalized through clathrin-mediated endocytosis on Wnt stimulation,[14,15] FZD10 may be also internalized with unknown ligands as well as MAb 92-13 although further studies will be required.

doi: 10.1111/j.1349-7006.2007.00701.x
© 2008 Japanese Cancer Association

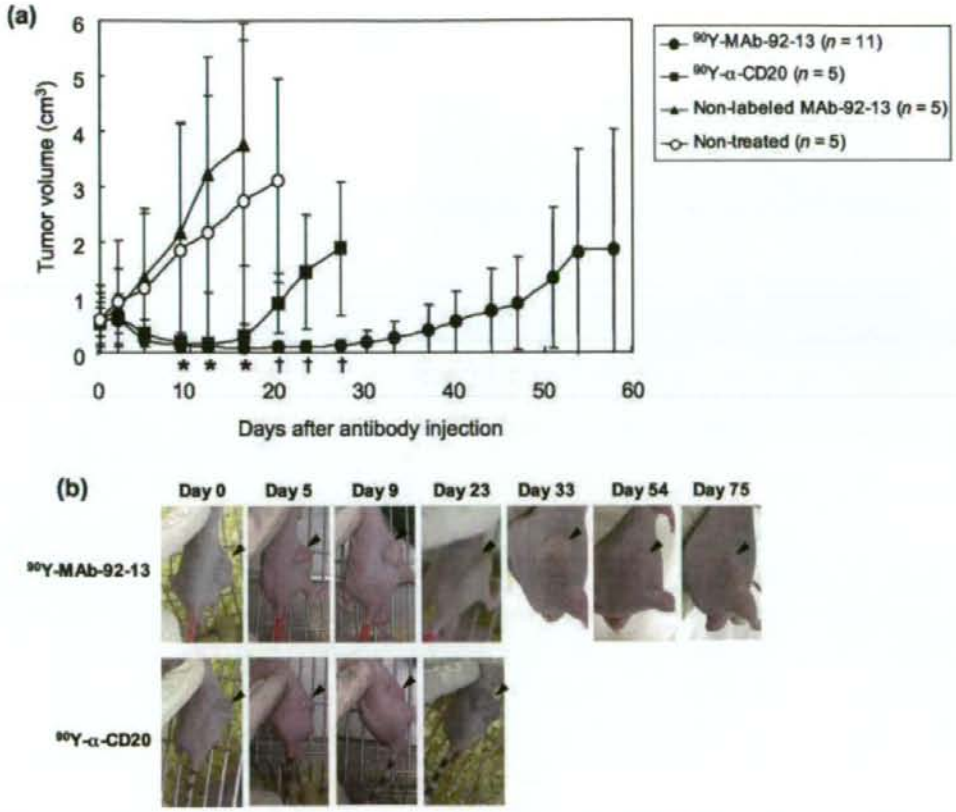

Fig. 5. Radioimmunotherapy in SYO-1-tumor bearing nude mice. (a) Balb/c nude mice bearing fully established (mean tumor volume = 0.56 cm^3) SYO-1 tumors were treated with Yttrium-90 (^{90}Y)-MAb 92-13 (n = 11), ^{90}Y-α-CD20 (n = 5), non-labeled MAb 92-13 (n = 5) or untreated (non-treated) (n = 5). Mice were given a single injection at day 0. The mean tumor volumes were plotted against days after the antibody injection (error bars are 95% confidence interval). Closed circle, ^{90}Y-MAb 92-13; closed square, ^{90}Y-α-CD20; closed triangle, non-labeled MAb 92-13; open circle, non-treated. Welch's two-sided Student's t-test was used for comparison with control mice, and statistically significant points ($P < 0.05$) are noted: *, vs non-labeled MAb 92-13; †, vs ^{90}Y-α-CD20. (b) Representative images of ^{90}Y-MAb 92-13-treated mice. The photographs of ^{90}Y-MAb 92-13-treated mice (upper panels) and ^{90}Y-α-CD20-treated mice (lower panels) were taken at the days indicated. Arrowheads indicate the tumor. Note that the tumor size was reduced in a mouse treated with ^{90}Y-α-CD20 at day 5, but was increased again at day 9, while the tumor in that with ^{90}Y-MAb 92-13 diminished completely at day 33, and showed no regrowth at day 75.

Zevalin (anti-CD20 antibody conjugated with ^{90}Y) has been proven to provide a new means of cancer treatment called radioimmunotherapy and, in fact, has been highly effective against malignant lymphoma.[16] We confirmed that MAb 92-13 had no antitumor activity *in vitro* when treated to FZD10-overexressing cells, SYO-1 (data not shown). However, because we observed the effective internalization and accumulation of MAb 92-13 into the synovial sarcoma cells as shown in Figures 3 and 4, we, in this study, designed the radioimmunotherapy using ^{90}Y-conjugated MAb 92-13 for treatment of synovial sarcomas. In the mouse xenograft model, tumors rapidly diminished after the single treatment of ^{90}Y-MAb 92-13 and no toxicity was observed. Because MAb 92-13 was internalized effectively into antigen-positive cells as described above, conjugation of anticancer drugs to MAb 92-13 may also be expected to exert the high anticancer effect to synovial sarcoma cell as well as ^{90}Y-MAb 92-13.

In conclusion, we successfully generated a monoclonal antibody, which specifically bound to FZD10 *in vitro* and *in vivo*, and was internalized into and accumulated in FZD10-expressing cells. A single i.v. injection of radioisotope-labeled MAb 92-13 showed strong antitumor activity *in vivo*. Taken together, we are confident that anti-FZD10 antibody MAb 92-13 has a great potential for development of a novel treatment of synovial sarcoma as well as other tumors that show overexpression of FZD10. Interestingly, our cDNA microarray data and immunohistochemical staining analysis showed the upregulation of FZD10 in a subset of colon cancer, lung cancer and gastric cancer (data not shown). Hence, this antibody treatment might be applied to a wide range of cancer types.

Acknowledgments

We thank Chiyoda Technol for providing ^{90}Yttrium solution, Dr Ryo Takata for statistical analysis, and Ms Kie Naito, Ms Yoshiko Fujisawa, Ms Kyoko Kijima, Ms Akiko Konuma and Ms Aya Sasaki for excellent technical assistance. All authors have contributed significantly, and are in agreement with the content of this manuscript.

© 2008 Japanese Cancer Association

References

1 Harris M. Monoclonal antibodies as therapeutic agents for cancer. *Lancet Oncol* 2004; **5**: 292–302.
2 Baselga J. Herceptin® alone or in combination with chemotherapy in the treatment of HER2-positive metastatic breast cancer: pivotal trials. *Oncology* 2001; **61** (Suppl 2): 14–21.
3 Maloney DG, Grillo-López AJ, White CA *et al*. IDEC-C2B8 (Rituximab) Anti-CD20 monoclonal antibody therapy in patients with relapsed low-grade non-Hodgkin's lymphoma. *Blood* 1997; **90**: 2188–95.
4 Ferrara N, Hillan KJ, Gerber HP, Novotny W. Discovery and development of bevacizumab, an anti-VEGF antibody for treating cancer. *Nat Rev Drug Discov* 2004; **3**: 391–400.
5 Crist WM, Anderson JR, Meza JL *et al*. Intergroup rhabdomyosarcoma study-IV. results for patients with nonmetastatic disease. *J Clin Oncol* 2001; **19**: 3091–102.
6 Ferguson WS, Goorin AM. Current treatment of osteosarcoma. *Cancer Invest* 2001; **19**: 292–315.
7 Wunder JS, Paulian G, Huvos AG, Heller G, Meyers PA, Healey JH. The histological response to chemotherapy as a predictor of the oncological outcome of operative treatment of Ewing sarcoma. *J Bone Joint Surg Am* 1998; **80**: 1020–33.
8 Nagayama S, Katagiri T, Tsunoda T *et al*. Genome-wide analysis of gene expression in synovial sarcomas using a cDNA Microarray. *Cancer Res* 2002; **62**: 5859–66.
9 Koike J, Takagi A, Miwa T, Hirai M, Terada M, Katoh M. Molecular cloning of *Frizzled-10*, a novel member of the *Frizzled* gene family. *Biochem Biophys Res Commun* 1999; **262**: 39–43.
10 Nagayama S, Fukukawa C, Katagiri T *et al*. Therapeutic potential of antibodies against FZD10, a cell-surface protein, for synovial sarcomas. *Oncogene* 2005; **24**: 6201–12.
11 Arano Y, Fujioka Y, Akizawa H *et al*. Chemical design of radiolabeled antibody fragments for low renal radioactivity levels. *Cancer Res* 1999; **59**: 128–34.
12 Arpino G, Gutierrez C, Weiss H *et al*. Treatment of human epidermal growth factor receptor 2-overexpressing breast cancer xenografts with multiagent HER-targeted therapy. *J Natl Cancer Inst* 2007; **99**: 694–705.
13 Chen X, Conti PS, Moats R. *In vivo* near-infrared fluorescence imaging of integrin αvβ3 in brain tumor xenografts. *Cancer Res* 2004; **64**: 8009–14.
14 Chen W, ten Berge D, Brown J *et al*. Dishevelled 2 recruits β-arrestin 2 to mediate Wnt5A-stimulated endocytosis of Frizzled 4. *Science* 2003; **301**: 1391–4.
15 Bryja V, Cajánek L, Grahn A, Schulte G. Inhibition of endocytosis blocks Wnt signaling to β-catenin by promoting disheveled degradation. *Acta Physiol* 2007; **190**: 55–61.
16 Wiseman GA, Witzig TE. Yttrium-90 (^{90}Y) ibritumomab tiuxetan (Zevalin) induces long-term durable responses in patients with relapsed or refractory B-cell non-Hodgkin's lymphoma. *Cancer Biother Radiopharm* 2005; **20**: 185–8.

Appendix I

The following supplementary material is available for this article.

Figure S1. Specificity of ^{111}In-labeled MAb 92-13 accumulation to SYO-1-tumor xenografts. Radiolabeled MAb 92-13 was injected s.c. to SYO-1-tumor bearing mice in the absence or presence of non-labeled MAb 92-13, respectively. The normal organs (blood, liver, kidney, intestine, spleen, pancreas, lung, heart, stomach and muscle) and tumor were dissected at 48 h after the injection with ^{111}In-MAb 92-13, and the radioactivities were measured. The data shown are the representative data in two independent experiments. Open bar, SYO-1-tumor bearing mice injected with only ^{111}In-MAb 92-13; closed bar, SYO-1-tumor bearing mice pre-injected with non-labeled MAb 92-13.

Figure S2. Bodyweight of mice received radioimmunotherapy. Tumor-bearing BALB/c nude mice treated with ^{90}Y-MAb 92-13 or non-labeled MAb 92-13, or those without any treatments were weighed at the days indicated. The mean values of each group are plotted. Closed circle, ^{90}Y-MAb 92-13; closed square, ^{90}Y-α-CD20; closed triangle, non-labeled MAb 92-13; open circle, non-treated.

Figure S3. Binding of ^{125}I-labeled MAb 92-13 to normal human blood cells. Radiolabeled MAb 92-13 was incubated with normal human fresh blood of three individuals (donors A, B and C) in the absence or presence of non-labeled MAb 92-13, respectively. Closed bars, ^{125}I-MAb 92-13; open bars, ^{125}I-MAb 92-13 + non-labeled MAb 92-13.

This material is available as part of the online article from: http://www.blackwell-synergy.com/doi/abs/10.1111/j.1349-7006.2008.00701.x (this link will take you to the article abstract).

Please note: Blackwell Publishing are not responsible for the content or functionality of any supplementary materials supplied by the authors. Any queries (other than missing material) should be directed to the corresponding author for the article.

doi: 10.1111/j.1349-7006.2007.00701.x
© 2008 Japanese Cancer Association

Lung Cancer (2008) 59, 203–210

available at www.sciencedirect.com

ScienceDirect

journal homepage: www.elsevier.com/locate/lungcan

Usefulness of FDG-PET for early prediction of the response to gefitinib in non-small cell lung cancer

Noriaki Sunaga[a,*], Noboru Oriuchi[b], Kyoichi Kaira[a], Noriko Yanagitani[a], Yoshio Tomizawa[a], Takeshi Hisada[a], Tamotsu Ishizuka[a], Keigo Endo[b], Masatomo Mori[a]

[a] *Department of Medicine and Molecular Science, Gunma University Graduate School of Medicine, 39-15 Showa-machi 3-chome, Maebashi, Gunma 371-8511, Japan*
[b] *Department of Diagnostic Radiology and Nuclear Medicine, Gunma University Graduate School of Medicine, 39-15 Showa-machi 3-chome, Maebashi, Gunma 371-8511, Japan*

Received 18 May 2007; received in revised form 26 July 2007; accepted 12 August 2007

KEYWORDS
Non-small cell lung cancer;
Gefitinib;
Fluorodeoxyglucose;
Positron emission tomography

Summary Increased tumor uptake of ^{18}F-fluorodeoxyglucose (FDG) measured by positron emission tomography (PET) reflects glucose metabolism and proliferative activity of tumor cells. We conducted a study to assess the usefulness of FDG-PET for early prediction of the response to gefitinib, an epidermal growth factor receptor (EGFR) tyrosine kinase inhibitor (TKI), in advanced non-small cell lung cancer (NSCLC). Five NSCLC patients underwent FDG-PET to evaluate changes in FDG uptake at day 2 and 4 weeks after the initiation of gefitinib therapy compared with FDG-PET prior to therapy. FDG uptake was evaluated as the maximum standardized uptake value (SUVmax) of the target lesions, which were assessable by conventional CT. Based on the CT evaluation, two patients exhibited a partial response (PR), two patients had stable disease (SD) with a minor response, and one patient had progressive disease (PD). In patients with PR and SD, SUVmax decreased by $61 \pm 18\%$ (standard deviation) and $59 \pm 12\%$, respectively, on day 2, and by 26 ± 6 and $43 \pm 10\%$, respectively, at 4 weeks after the initiation of gefitinib. Two patients with SD had decreased FDG uptake within 2 days of initiation of therapy, and achieved progression-free survival (PFS) of more than 12 months. In contrast, SUVmax increased up to $153 \pm 21\%$ at 2 days and $232 \pm 73\%$ at 4 weeks in a patient with PD. The present preliminary study suggests that FDG-PET may be able to predict response to gefitinib in the early stage of therapy in patients with advanced NSCLC and may have a potential prognostic role.
© 2007 Elsevier Ireland Ltd. All rights reserved.

* Corresponding author. Tel.: +81 27 220 8136; fax: +81 27 220 8136.
E-mail address: nsunaga@showa.gunma-u.ac.jp (N. Sunaga).

0169-5002/$ – see front matter © 2007 Elsevier Ireland Ltd. All rights reserved.
doi:10.1016/j.lungcan.2007.08.012